

A Nonlinear Analysis of the ENSO Cycle and Its Interdecadal Changes

Soon-Il An

International Pacific Research Center, University of Hawaii at Manoa, Honolulu, Hawaii

William W. Hsieh

Department of Earth and Ocean Sciences, University of British Columbia, Vancouver,
British Columbia, Canada

Fei-Fei Jin

Department of Meteorology, Florida State University, Tallahassee, Florida

Jan, 2005

J. Climate

Corresponding author address: Dr. Soon-Il An, International Pacific Research Center,
SOEST, University of Hawaii at Manoa, Honolulu, HI 96822. E-mail: sian@hawaii.edu

Abstract

The nonlinear principal component analysis (NLPCA), via a neural network approach, was applied to the thermocline anomalies in the tropical Pacific. While the tropical sea surface temperature (SST) anomalies had been nonlinearly mapped by the NLPCA mode 1 onto an open curve in the data space, the thermocline anomalies were mapped to a closed curve, suggesting that ENSO is a cyclic phenomenon. The NLPCA mode 1 of the thermocline anomalies reveals the nonlinear evolution of the ENSO cycle with much asymmetry for the different phases: The weak heat accumulation in the whole equatorial Pacific is followed by the strong El Niño, and the subsequent strong drain of equatorial heat content toward the off-equatorial region precedes a weak La Niña. This asymmetric ENSO evolution implies that the nonlinear instability enhances the growth of El Niño, but dwarfs the growth of La Niña. The nonlinear ENSO cycle was found to have changed since the late 1970s. For the pre-1980s, the ENSO cycle associated with the thermocline is less asymmetrical than that during the post-1980s, indicating that the nonlinearity of the ENSO cycle has become stronger since the late 1970s.

1. Introduction

Despite numerous investigations into the mechanism of the El Niño-Southern Oscillation (ENSO) (see, for example, 'Reviewing the progress of El Niño research and prediction' in a special volume of *J. Geophys. Res.*, **103**, 1998), the climate study community still does not have a consensus on some intrinsic questions: the first question is whether ENSO is a large-scale deterministic system, the apparently random behavior of which can be explained by nonlinear dynamics (Jin et al. 1994; Tziperman et al. 1994) or whether ENSO is linear, the erratic behavior of which is caused by stochastic forcing (Penland and Sardeshmukh 1995; Chang et al. 1996; Moore and Kleeman 1999; Thompson and Battisti 2000, 2001); the second question is whether ENSO is cyclic or sporadic (e.g., Kessler 2002, Philander and Fedorov 2003). These two questions are not simply independent but should be considered in parallel. This is because the linear system subjected to stochastic forcing is more likely to produce a sporadic ENSO, while the deterministic system with the strong nonlinearity is more likely to produce a cyclic ENSO.

Thompson and Battisti (2001) stochastically forced a linear model that originally does not sustain internally generated variability, and found that it reproduces all of the basic features of ENSO, suggesting that the essential characteristics of ENSO appear to be governed by linear processes, but it failed to produce the significant positive skewness of the ENSO index. On the contrary, several observational studies point out that the probability density function of ENSO indices (i.e., Niño-1, 2, 3, 3.4) are distinguishable from a Gaussian

distribution, and the positively skewed SST anomalies over the eastern Pacific are caused by the nonlinearity (Burgers and Stephenson 1999; Hannachi et al. 2003; Jin et al. 2003; An and Jin 2004). In particular, Jin et al. (2003) introduced a dynamical measure of ENSO nonlinearity (i.e. 'nonlinear dynamical heating'; NDH) along with a statistical measure such as skewness. They concluded that the NDH could cause the positively skewed SST anomalies over the eastern Pacific.

To identify the principal mode associated with tropical Pacific interannual variability, traditional statistical methods such as the principal component analysis (PCA, a.k.a. empirical orthogonal function analysis; EOF) or the maximum covariance analysis (MCA, a.k.a. singular value decomposition; SVD) were widely used. These linear methods obviously identify the most dominant pattern associated with ENSO, in which the spatial pattern associated with El Niño is exactly the same as that associated with La Niña but of an opposite sign. However, in reality the spatial patterns associated with El Niño and La Niña are not identical due to the nonlinearity (Hoerling et al. 1997; Monahan 2001). Recently, using nonlinear principal component analysis (NLPCA), which detects a low-dimensional nonlinear structure in multivariate datasets, Hsieh (2001, 2004) objectively characterized the asymmetric features between El Niño and La Niña. The nonlinear principal mode showed that not only the amplitude of El Niño is larger than that of La Niña, but also the maximum sea surface temperature (SST) of El Niño is confined to the eastern equatorial Pacific, while the minimum of La Niña is located at the central equatorial Pacific.

While PCA finds a straight line that passes through the 'middle' of the data cluster, a nonlinear mapping of NLPCA possibly replaces the straight line by a continuous open or closed curve for approximating the data (Hsieh 2004). As an open curve solution, for example, a U-shaped curve solution nonlinearly connects two extreme states. On the other hand, a quasi-periodic geophysical phenomenon may call for the closed curve solution. For example, Hamilton and Hsieh (2002) applied the NLPCA to the stratospheric equatorial zonal wind data to study the quasi-biennial oscillation and found a closed curve solution.

Monahan (2001) and Hsieh (2001) applied the NLPCA to tropical Pacific SST anomalies to reveal the nonlinear principal mode of ENSO. Despite ENSO's quasi-oscillatory behavior, the mapped curve turned out to be a U-shaped curve, which links La Niña states at one end to the El Niño states at the other end. In other words, the pathway from El Niño to La Niña is similar to that from La Niña to El Niño. This is because the SST patterns during the transition phase do not change much depending on whether El Niño proceeds to La Niña or the other way around. On the other hand, the oceanic heat content (with the thermocline as a proxy) clearly shows a complete cyclic feature for ENSO shown in observation (Jin and An 1999; Meinen and McPhaden 2000) and the ocean-atmosphere coupled general circulation model (CGCM) (Mechoso et al. 2003), because the thermocline depth during the transition phase from El Niño to La Niña is shallow over the entire equatorial Pacific, while that during the transition phase from La Niña to El Niño is deeper. Thus, in this study, by using NLPCA,

we will identify the cyclic feature of ENSO, and also explore the nonlinearity of ENSO.

In section 2, we describe the data and the analysis method. Section 3 presents the NLPCA modes of the thermocline anomalies to reveal the ENSO cycle with a nonlinear behavior. In section 4, we compare the NLPCA modes of the thermocline before and after a “climate regime” shift since the late 1970s to explore the nonlinear interdecadal changes in the ENSO cycle. Summary and discussion are given in Section 5.

2. Data and Method

The data utilized are the National Center for Environmental Prediction (NCEP) ocean assimilation data for Jan. 1980 – Oct. 2000 (Ji et al. 1995; Behringer et al. 1998; Vossepoel and Behringer 2000). Observed surface and subsurface ocean temperatures as well as satellite altimetry sea-level data from TOPEX/POSEIDON were assimilated into a Pacific Ocean general circulation model. The model was forced with weekly-mean surface winds and heat fluxes of NCEP operational atmospheric analyses. This data set has 16 levels in the upper 200m, where the interval between levels is around 10-30 m. From the temperature data, the depth of the 20 °C isotherm has been calculated. This isotherm is used as a proxy for the total heat content.

We also used the simple ocean data assimilation (SODA) set (Carton et al. 2000), for investigating the long-term change and comparing with the NCEP data. The SODA data (Jan. 1950 to Dec. 2001) were built by interpolating

unevenly distributed ocean measurements into three-dimensional global fields of temperature, salinity, and current velocity using an ocean general circulation model. The TOGA/TAO data and TOPEX/POSEIDON data were used for checking the quality of the SODA data set (e.g., Carton et al. 2000; Xie et al. 2002). Both NCEP and SODA data sets contain monthly-mean data.

In principal component analysis (PCA), also known as empirical orthogonal function analysis, a straight line approximation to the dataset is sought which accounts for the maximum amount of variance in the data. There are now several types of neural network (NN) models which use, instead of the straight line, a continuous curve to approximate the data (Hsieh, 2004). Using a multi-layer perceptron NN formulation, the nonlinear PCA (NLPCA) method of Kramer (1991) is capable of finding an open curve to approximate the data. However, for periodic or quasi-periodic phenomena, it would be more appropriate to fit the data with a closed curve instead of an open curve. Kirby and Miranda (1996) introduced an NLPCA variant, which has a circular bottleneck node, thereby allowing the extraction of closed curve solutions. This variant of NLPCA, used by Hsieh (2001) and Hamilton and Hsieh (2002) to study tropical climate variability, is the one used in this paper. For more details of the method, see the review paper by Hsieh (2004).

The input data are in the form $\mathbf{x}(t) = [x_1(t), \dots, x_l(t)]$, where each variable x_i ($i = 1, \dots, l$), is a time series containing n observations. To perform NLPCA (Fig. 1), the information is mapped forward through a bottleneck to the output \mathbf{x}' . The parameters of the network are solved by minimizing the cost function, which is

basically the mean square error (MSE) of \mathbf{x} relative to \mathbf{x}_c . Because of local minima in the cost function, an ensemble of 30 NNs with random initial weights and bias parameters was run. Also, 15% of the data was randomly selected as test data and withheld from the training of the NNs. Runs where the MSE was larger for the test dataset than for the training dataset were rejected to avoid overfitted solutions. Then the NN with the smallest MSE was selected as the solution.

The gridded 20 °C thermocline data were linearly detrended, then reduced by PCA to 5 leading principal component (PC) time series. These 5 PCs then become the input $\mathbf{x}(t) = [x_1(t), \dots, x_5(t)]$ of the NLPCA network. The number of model parameters (i.e. weights) is controlled by m , the number of nodes in the encoding layer (and in the decoding layer). Excessive m and excessively large weights can lead to over-fitting. A weight penalty term is added to the cost function to avoid excessively large weights (see Hsieh, 2001 or Hsieh, 2004, with the weight penalty parameter being 1). Also, m was varied between 2 and 8, and the one giving the lowest MSE was selected.

3. NLPCA mode of tropical Pacific thermocline

We have applied PCA to the 21-year monthly-mean 20 °C isotherm depth anomalies (a proxy of the thermocline depth) obtained from NCEP ocean assimilation data (Ji et al. 1995), where to determine the anomalies, the 21-year climatological monthly mean and the linear trend were removed. In Fig. 2, the dominant feature of the thermocline anomaly is summarized by the two leading

PCA modes: the first mode is a zonal contrast mode and the second mode has a strong zonal-symmetric component. Two leading PCA modes explain 31% and 22% of total variance, respectively. The first mode varies in-phase with ENSO (where ENSO is represented by the Niño-3 index), and its amplitude is linearly proportional to the ENSO amplitude. The second mode leads ENSO by a quarter cycle. Those features are similar to that described by a recharge paradigm under the linear dynamical framework (Jin 1997a, b). However, the amplitude of the second mode is not simply proportional to the amplitude of the following ENSO, indicating the linear mechanism may not be enough to explain this thoroughly. In this section, we identify the principal patterns of the thermocline variation by using NLPCA, which provides a much clearer idea about the nonlinearly related patterns.

From the first 5 leading PCA modes of the thermocline anomalies, we extracted the NLPCA mode. Here, the first NLPCA explains 48% of total variance. In Fig. 3, NLPCA gives a continuous closed curve solution in the 5-dimensional space (here, we only draw the curve in the 3-dimensional space as shown in Fig. 3b), as the nonlinear principal component $\theta(t)$ is an angular variable. The system generally progresses clockwise along the closed curve in Fig. 3a with the upper- and lowermost points of the curve corresponding to the transition phase from La Niña to El Niño and that from El Niño to La Niña, respectively. Since the data are approximated by a closed continuous curve, the thermocline anomalies are dominated by a quasi-periodic fluctuation, and thus ENSO may be considered as an oscillatory mode. However, the amplitude

moving from one phase of the cycle to another is asymmetric. Likewise, the center of the closed curve in Fig. 3a is not located at the center of the diagram. The amplitude of the recharge (top of curve) associated with a subsequent El Niño (right side of curve, with a large amplitude) is smaller than that of the discharge (bottom of curve) associated with a subsequent La Niña (left side of curve, with a small amplitude). This asymmetry was also mentioned by Meinen and McPhaden (2000), who examined 18 years of surface temperature data. Note that the data points are strongly scattered about the curve in Fig. 3a during the transition from La Niña to El Niño (associated with the recharge period of total heat content), while they fit closely to the curve during the transition from El Niño to La Niño (associated with the discharge period of total heat content), suggesting that stochastic variability may be more active for the La Niña-to-El Niño transition.

To show the spatial distribution of the thermocline associated with the ENSO cycle, we draw the NLPCA mode 1 with a quarter cycle interval in Fig. 4: the mature phase of El Niño (Fig. 4a), transition phase from El Niño to La Niña (Fig. 4b), mature phase of La Niña (Fig. 4c), and transition phase from La Niña to El Niño (Fig. 4d). For the mature phase of El Niño, there are large positive anomalies over the eastern tropical Pacific centered near the eastern boundary, and large negative anomalies over the western tropical Pacific centered near the western boundary. This zonal contrast pattern of thermocline obviously leads to strong poleward geostrophic transport, resulting in the strong discharge of the equatorial total heat content. Consequently, for the transition phase from El Niño

to La Niña, the thermocline depth becomes considerably shallower over the whole equatorial Pacific. This shoaling thermocline presumably leads to the La Niña. During La Niña, the zonal contrast of the thermocline has an opposite sign to that during El Niño, and its strength is about half of that during El Niño. This results in the weak equatorward heat transport. Thus, the recharge of the equatorial total heat content is relatively weaker than the discharge (also see Fig. 3a). Observationally, La Niña tends to strictly follow El Niño (e.g., the 1982-83 El Niño is followed by the 1983-84 La Niña, and the 1997-98 El Niño is followed by the 1998-99 La Niña), whereas the recharge process that possibly leads to the transition from La Niña to El Niño is relative weak. Kessler (2002) even argued for a distinct break in the ENSO cycle, especially when it goes from La Niña to El Niño. We will get to this point in section 5.

Figure 5 shows the propagation feature of the thermocline anomalies associated with the dominant nonlinear ENSO cycle over the equator, as well as the associated surface wind stress anomalies. The surface wind stress data are obtained from Florida State University (Goldenberg and O'Brien 1981). This pattern is again obtained from the NLPCA mode 1. During El Niño, the positive maximum thermocline appears at the far eastern Pacific near 90° W, while during the La Niña the maximum negative thermocline appears at the central-eastern Pacific near 120° W. In other words, the maximum for the El Niño anomaly tends to shift to the east compared to that for the La Niña. This difference in the zonal location may be related to the difference in the location of the anomalous atmospheric heating – the equatorial central Pacific for El Niño and the western

Pacific for La Niña – causing the surface wind to be located differently as shown in Fig. 5. It is known that the thermocline variation in the equatorial western Pacific is transmitted to the equatorial eastern Pacific through the equatorial waveguide (Wyrtki 1985). For La Niña, the amplitude of the negative thermocline in the equatorial central-eastern Pacific is almost equal to that in the western Pacific during the previous El Niño, whereas for the El Niño, the positive thermocline anomaly in the equatorial eastern Pacific is 4 times that of the positive anomaly in the western Pacific during the previous La Niña. Thus, the thermocline variation during La Niña seems to be totally drained from the western Pacific thermocline anomaly that was built during the previous El Niño. In other words, the weak preconditioning for El Niño through recharge process and rapid growth of the El Niño, in contrast to the relative strong preconditioning for La Niña through strong discharge process and weak growth of La Niña, indicates that El Niño may be less predictable than La Niña.

To examine the evolution of the total heat content, we show the phase-latitude section of the zonal-mean thermocline anomalies associated with the NLPCA mode 1 in Fig. 6. A strong asymmetry between the recharge and discharge is pronounced. The discharge process indicating the loss of the equatorial heat content and the gain of the off-equatorial heat content seems to agree well with the recharge paradigm (Jin 1997a, b), while the recharge process is relatively weak and less obvious. Not only the asymmetry between recharge and discharge, but also the north-south asymmetry during the discharge is observed such that there is a large heat content increase in the off-equatorial

North Pacific but not in the off-equatorial South Pacific. Kug et al. (2003) pointed out that the asymmetric poleward mass transports are due to a southward shift of the maximum zonal wind stress anomaly during the ENSO mature phase associated with the seasonal march of South Tropical Convergence Zone. The negative equatorial heat content lives longer than the positive heat content does, and the off-equatorial heat content is smaller in magnitude than the equatorial heat content for the discharge, while for the recharge, the opposite is true.

4. Interdecadal changes in the tropical Pacific thermocline evolution

Concurrent with the well-known climate shift, not only the general characteristics of ENSO such as the period, intensity, spatial pattern, propagating feature, and onset (Wang 1995; An and Jin 2000; An and Wang 2000; Wang and An 2001), but also the nonlinearity of ENSO has changed during the late 1970s (Jin et al. 2003; Wu and Hsieh 2003; An 2004; An and Jin 2004). After the 1980s, the skewness of the ENSO index (e.g., Nino-3 index) increased to being more positive so that the asymmetry between El Niño and La Niña also increased (Wu and Hsieh 2003; An 2004). An and Jin (2004) pointed out that the asymmetry of ENSO was due to the nonlinear dynamical heating, which also increased after the late 1970s. Naturally, this inspires us to explore the interdecadal change in the nonlinear ENSO cycle.

The NCEP ocean assimilation data only cover the recent 20 years, too short for the interdecadal study. Instead, we use the SODA data, which cover over 50 years. A cross-check between two data sets for the recent 20 years also

gives us confidence in our results. Again PCA was applied to the 20 °C isotherm anomalies, and the PCs of the first 5 leading modes were used for the further application. The leading PCA patterns are in general similar to those obtained from NCEP ocean assimilation data (not shown here). Next, we divided the whole period into two parts – one for 1950-1975 and the other for 1980-2001 – and calculated the NLPCA mode of the thermocline anomalies for each period and for the whole period as well.

Fig. 7 shows a scatter plot in the PC1-PC2 plane for NLPCA mode 1 for each different period. First of all, we found that the scatter plot for SODA data (Fig. 7c) is similar to that for NCEP data (Fig. 3), which verifies the robustness of the result. The closed curve for the pre-1980s (Fig. 7b) is less asymmetrical than that for the post-1980s (Fig. 7c). For the pre-1980s (Fig. 7b), the recharged total heat content (lowermost part) is slightly larger than the discharged total heat content (uppermost part), and the La Niña pattern (the left end) is also slightly stronger than the El Niño pattern (the right end). These decadal changes are consistent with the changes in the skewness and nonlinearity of ENSO, which has increased since the late 1970s. For the total period, the closed curve in the PC1-PC2 plane (Fig. 7a) shows a rather symmetrical circle, indicating that the canonical feature of ENSO is quite symmetrical. In other words, the canonical ENSO resembles the recharge paradigm, but ENSO in each interdecadal period has its own characteristics, which is mainly due to the interdecadal changes in the nonlinearity of ENSO.

We show the evolution feature of the thermocline anomalies obtained from the NLPCA mode 1 along the equator and associated surface wind stress anomalies in Fig. 8. Again, for the post-1980s, the result of SODA (Fig. 8c) and that of NCEP (Fig. 5) data are similar in quality. The difference in quantity is presumably due to difference in the assimilation method or difference in the climatologically mean used for the anomaly calculation. Interestingly, the negative center of the thermocline anomaly for the post-1980s is confined over the central equatorial Pacific, which is stronger than the positive thermocline anomaly over the eastern Pacific, whereas for the pre-1980s there are two negative thermocline anomaly centers (in the western equatorial Pacific and the eastern Pacific) of which the amplitudes are slightly smaller than the positive thermocline anomalies. Also the positive and negative centers are located at the same longitude in the eastern and western Pacific for the pre-1980s.

The interdecadal change in the thermocline observed here is dynamically consistent with the interdecadal changes in the surface wind. As shown in Fig. 8, as well as in Wu and Hsieh (2003), for the pre-1980s the surface wind stress anomaly for El Niño is slightly smaller than that for La Niña with the opposite sign, while for the post-1980s, the surface wind anomaly for El Niño has a larger amplitude and its zonal location is shifted eastward relative to that for La Niña. Since the surface wind stress patterns for El Niño and La Niña are more or less symmetrical in their longitudes for the pre-1980s, the thermocline patterns for El Niño and La Niña are also similar. On the other hand, for the post-1980s, the longitudinal distribution of the thermocline shifts to the east and the zonal

contrast becomes stronger during El Niño, because of the stronger surface wind stress and the eastward shift of the surface wind stress pattern during El Niño. The eastward shift in the dominant pattern of surface wind stress anomalies associated with ENSO since the late 1970s, as shown in An and Wang (2000), might be due to the increase of nonlinearity of ENSO. In particular, the surface wind associated with El Niño was significantly shifted eastward, while that associated with La Niña was not changed much. Note that the canonical feature of thermocline evolution shown in Fig. 8a is again more likely symmetric, similar to the pattern shown in the theoretical studies (e.g., Jin 1997a, b; Jin and An 1999).

To detect interdecadal changes in the evolution of the total heat content, we plotted the phase-latitude section of the zonal-mean thermocline anomalies associated with the NLPCA mode 1 for the each period in Fig. 9. One observes that the SODA result (Fig. 9c) is consistent with the NCEP result (Fig. 6). In contrast to the post-1980s, the warm period of the total heat content on the equator during the pre-1980s is relatively longer than the cold period of the total heat content; the warming of the total heat content is stronger than the cooling; and the accumulation of the off-equatorial total heat content is weak, so that the total heat content anomalies for the pre-1980s seem to vary only over the equatorial region. The equatorial total heat content anomalies for the pre-1980s is positively skewed, while that for the post-1980s is negatively skewed in terms of both the amplitude and duration period. However, the canonical pattern of the

total heat content anomalies (Fig. 9a) shows symmetry in terms of the period and the amplitude due to a linear combination of two inversely skewed patterns.

5. Summary and discussion

PCA (and rotated PCA) have been widely used to extract the optimal linear structure from a dataset. When the dataset has an underlying structure which is not linear, NLPCA may provide a better way to describe the dataset. By applying NLPCA to the thermocline anomalies in the tropical Pacific, we have identified an ENSO cycle with notable nonlinearity. Although previous applications of NLPCA to the SST anomalies have only found a U-shaped open curve as the best fit to the data, in this study the NLPCA mode of the thermocline anomalies reveals a closed curve. In an open-curve solution, the transition from El Niño to La Niña is indistinguishable from the reverse transition from La Niña to El Niño, whereas in a closed-curve solution, the two transitions are distinct. Interestingly, this closed curve of the NLPCA mode 1 shows an asymmetry feature: A weak recharge of the equatorial zonal mean thermocline precedes the steep zonal slope of anomalous thermocline downward to the east along the equator (strong El Niño), and the subsequent strong discharge is followed by a gentle zonal slope of anomalous thermocline downward to the west (weak La Niña). The strong drain of the equatorial total heat content is probably enough to suppress El Niño, and afterward to lead to La Niña. Since the discharge process drives a strong shoaling of thermocline, one may expect a strong La Niña in a linear sense. However, the La Niña cannot grow as much as expected because

the nonlinear dynamical heating dwarfs the growth of La Niña (Jin et al. 2003; An and Jin 2004). On the contrary, the increase of the total heat content due to the recharge process is weak, but the nonlinear dynamic heating intensifies the El Niño, resulting in the strong El Niño. In particular, the scatter from the regular orbit is more pronounced during the transition phase from La Niña to El Niño suggesting that other factors - including the stochastic forcing - strongly agitate the nonlinear ENSO cycle, presumably making the initiation of El Niño due to the heat accumulation over the tropical Pacific less obvious. In other words, there is asymmetry in the preconditioning of El Niño and La Niña events due to the asymmetry of recharge and discharge processes associated with nonlinear cycle of the ENSO. A linear stochastic forced system normally would not be able to produce such an asymmetry. In summary, ENSO appears to correspond to a nonlinear cyclic phenomenon and its erratic behavior is caused by the other factors including the stochastic forcing. We also found that the ENSO cycle has changed since the late 1970s. For the pre-1980s, the ENSO cycle associated with the thermocline is less asymmetric than that during the post-1980s; hence the nonlinearity of the ENSO cycle has become stronger since the late 1970s.

In this study, the nonlinear nature of the ENSO cycle obtained from NLPCA is simply identified as a closed curve approximating a relatively small amount of data in the linear PC space. Due to the insufficient data, it is hard to ensure that the decadal changes observed are real and not due to sampling uncertainty. Nevertheless, first, the NLPCA curves obtained from two different data sets (NCEP and SODA) showed a similar oblique pattern, and second, the

interdecadal change of ENSO observed in this study are dynamically consistent with other studies (e.g., Jin et al. 2003; An and Jin 2004, etc) that took different approaches.

Recently some observational studies have pointed out that while the termination of El Niño has occurred consistently with a cyclic nature, initiation is less obvious (Kessler and McPhaden, 1995; Kessler 2002), and some studies even concluded that ENSO is most likely a damped linear system subjected to stochastic forcing (Thompson and Battisti 2000, 2001). This linear approach succeeds in producing a sporadic ENSO but fails to produce the asymmetry of ENSO, since the nonlinear process is not included in the system. Apart from the additive stochastic forced system like Thompson and Battisti's model, the multiplicative stochastic forced system may induce the asymmetric probability density function for ENSO index. However, the asymmetric behaviors in the multiplicative stochastic forced system come from nonlinear process.

A kind of break in the ENSO cycle has been observed when La Niña goes to El Niño, during which the coupled system somehow remains in a weak La Niña state for a while (Kessler 2002). On one hand, this break in the ENSO cycle may be due to the influence of a near-annual mode. The near-annual mode is a unique air-sea coupled mode with a near-annual timescale apart from ENSO and is mainly induced by the zonal advection of mean SST by the anomalous zonal current (Jin et al. 2003; Kang et al. 2004). During La Niña the zonal contrast of equatorial SST becomes larger, which provides favorable condition for generating the near-annual mode, so that the oceanic memory built in a

sequence of the ENSO cycle is possibly contaminated by this near-annual mode. Thus, the isolation of the pure ENSO cycle from this near-annual signal should give a clearer picture. On the other hand, Yu et al. (2003) suggested that the westerly wind bursts (WWB) in the western equatorial Pacific, which had been considered as an important trigger of El Niño, could be regulated by ENSO in their generation such that the pre-El Niño state provides a favorable background condition on which the active WWB are generated, and consequently the ENSO cycle inherently has an ability to trigger itself. Their suggestion can be considered as a multiplicative stochastic system, in which the ENSO cycle interacts with the stochastic forcing. Regarding this topic, further studies need to be pursued.

Acknowledgments

This work is supported by National Science Foundation grant ATM-0226141 and by National Oceanographic and Atmospheric Administration grant GC01-229 and GC01-246. S.-I. An is supported by the Japan Agency for Marine-Earth Science and Technology (JAMSTEC) through its sponsorship of the International Pacific Research Center. W. Hsieh is supported by the Natural Sciences and Engineering Research Council of Canada and the Canadian Foundation for Climate and Atmospheric Sciences. The authors thank Diane Henderson for the careful reading and editing of the manuscript. SOEST contribution xxxx and IPRC contribution IPRC-yyy.

Reference

- An, S.-I., 2004: Interdecadal changes in the El Niño-La Niña asymmetry. *Geophys. Res. Lett.*, **31**, L23210, doi:10.1029/2004GL021699.
- An, S.-I., and F.-F. Jin, 2004: Nonlinearity and asymmetry of ENSO. *J. Climate*, **17**, 2399-2412.
- An, S.-I., and F.-F. Jin, 2001: Collective role of thermocline and zonal advective feedbacks in the ENSO mode. *J. Climate*, **14**, 3421-3432.
- An, S.-I., and F.-F. Jin, 2000: An eigen analysis of the interdecadal changes in the structure and frequency of ENSO mode. *Geophys. Res. Lett.*, **27**, 1573-1576.
- An, S.-I., and B. Wang, 2000: Interdecadal change of the structure of the ENSO mode and its impact on the ENSO frequency. *J. Climate*, **13**, 2044-2055.
- Behringer, D. W., M. Ji, and A. Leetmaa, 1998: An improved coupled model for ENSO prediction and implication for ocean initialization, Part I: The ocean data assimilation system. *Mon. Wea. Rev.*, **126**, 1013-1021.
- Burgers, G., and D. B. Stephenson, 1999: The “Normality” of El Niño. *Geophys. Res. Lett.*, **26**, 1027-1030.
- Carton, J., G. Chepurin, X. Cao, and B. Giese, 2000: A simple ocean data assimilation analysis of the global upper ocean 1950-1995, Part 1: methodology. *J. Phys. Oceanogr.*, **30**, 294-309.
- Chang, P., L. Ji, H. Li, and M. Flugel, 1996: Chaotic dynamics versus stochastic processes in El Niño-Southern Oscillation in coupled ocean-atmosphere

- models. *Physica D*, **9**, 301-320.
- Golednberg, S., and J. O'Brien, 1981: Time and space variability of the tropical Pacific wind stress. *Mon. Wea. Rev.*, **109**, 1190-1207.
- Hamilton, K. and W. W. Hsieh, 2002: Representation of the QBO in the tropical stratospheric wind by nonlinear principal component analysis. *Journal of Geophysical Research* **107**, D15, ACL3-1-10.
- Hannachi, A., D. B. Stephenson, and K. R. Sperber, 2003: Probability-based methods for quantifying nonlinearity in the ENSO. *Clim. Dyn.* **20**, 241-256.
- Hoerling, M. P., A. Kumar, and M. Zhong, 1997: El Niño, La Niña, and the nonlinearity of their teleconnections. *J. Climate*, **10**, 1769-1786.
- Hsieh, W. W., 2001: Nonlinear principal component analysis by neural networks. *Tellus*, **53A**, 599-615.
- Hsieh, W. W., 2004: Nonlinear multivariate and time series analysis by neural network methods. *Reviews of Geophysics*, **42**, RG1003, doi:10.1029/2002RG000112.
- Ji, M., A. Leetmaa, and J. Derber, 1995: An ocean analysis system for seasonal to interannual climate studies. *Mon. Wea. Rev.*, **123**, 460-481.
- Jin, F.-F., 1997a: An equatorial ocean recharge paradigm for ENSO. Part I: Conceptual model. *J. Atmos. Sci.*, **54**, 811-829.
- Jin, F.-F., 1997b: An equatorial ocean recharge paradigm for ENSO. Part II: A stripped-down coupled model. *J. Atmos. Sci.*, **54**, 830-846.
- Jin, F.-F., and S.-I. An, 1999: Thermocline and zonal advective feedbacks within the equatorial ocean recharge oscillator model for ENSO. *Geophys. Res.*

- Lett.*, **26**, 2989-2992.
- Jin, F.-F., J.-S. Kug, S.-I. An, and I.-S. Kang, 2003: A near-annual coupled ocean-atmosphere mode in the equatorial Pacific Ocean, *Geophys. Res. Lett.*, **30(2)**, 1080, doi:10.1029/2002GL015983.
- Jin, F.-F., J. D. Neelin, and M. Ghil, 1994: El Niño on the devil's staircase: Annual subharmonic steps to chaos. *Science*, **264**, 70-72.
- Kang, I.-S., J.-S. Kug, S.-I. An, and F.-F. Jin, 2004: A near-annual Pacific Ocean basin mode, *J. Climate*, **17**, 2478-2488.
- Kessler, W. S., 2002: Is ENSO a cycle or a series of events? *Geophys. Res. Lett.*, **29**, 2125, doi:10.1029/2002GL015924.
- Kessler, W. S., and M. J. McPhaden, 1995: Oceanic equatorial waves and the 1991-1993 El Niño. *J. Climate*, **8**, 1757-1774.
- Kirby, M. J., and R. Miranda, 1996: Circular nodes in neural networks. *Neural Comp.*, **8**, 390-402.
- Kramer, M. A., 1991: Nonlinear principal component analysis using autoassociative neural networks, *AIChE Journal*, **37**, 233-243.
- Kug, J.-S., I.-S. Kang, and S.-I. An, 2003: Symmetric and anti-symmetric mass exchanges between the equatorial and off-equatorial Pacific associated with ENSO, *J. Geophys. Res. - Oceans*, **108(C8)**, 3284, doi:10.1029/2002JC001671.
- Mechoso, C. R., J. D. Neelin, and J.-Y. Yu, 2003: Testing Simple Models of ENSO. *J. Atmos. Sci.*, **60**, 305-318.

- Meinen, C. S., and M. J. McPhaden, 2000: Observations of warm water volume changes in the equatorial Pacific and their relationship to El Niño and La Niña. *J. Climate*, **13**, 3551-3559.
- Monahan, A. H., 2001: Nonlinear principal component analysis: Tropical Indo-Pacific sea surface temperature and sea level pressure. *J. Climate*, **14**, 219-233.
- Moore, A. M., and R. Kleeman, 1999: Stochastic forcing of ENSO by the intraseasonal oscillation. *J. Climate*, **12**, 1199-1220.
- Penland, C., and P. D. Sardeshmukh, 1995: The optimal growth of tropical sea surface temperature anomalies. *J. Climate*, **8**, 1999-2024.
- Philander, S. G., and A. Fedorov, 2003: Is El Niño sporadic or cyclic? *Annu. Rev. Earth Planet. Sci.*, **31**, 579-594.
- Thompson, C. J., and D. S. Battisti, 2000: A linear stochastic dynamical model of ENSO. Part I: Model development. *J. Climate*, **14**, 445-466.
- Thompson, C. J., and D. S. Battisti, 2001: A linear stochastic dynamical model of ENSO. Part II: Analysis. *J. Climate*, **14**, 445-466.
- Tziperman, E., L. Stone, M. Cane, and H. Jarosh, 1994: El Niño chaos: Overlapping of resonances between the seasonal cycle and the Pacific ocean-atmosphere oscillator. *Science*, **264**, 72-74.
- Vossepoel, F. C., and D. W. Behringer, 2000: Impact of sea level assimilation on salinity variability in the western equatorial Pacific. *J. Phys. Oceanogr.*, **30**, 1706-1721.

- Wang, B., 1995: Interdecadal changes in El Niño onset in the late four decades. *J. Climate*, **8**, 267-285.
- Wang, B., and S.-I. An, 2001: Why the properties of El Niño changed during the late 1970s. *Geophys. Res. Lett.*, **28**, 3709-3712.
- Wu, A., and W. W. Hsieh, 2003: Nonlinear interdecadal changes of the El Niño-Southern Oscillation, *Clim. Dyn.* **21**, 719-730.
- Wytki, K., 1985: Water displacements in the Pacific and the genesis of El Niño cycles. *J. Geophys. Res.*, **90**, 7129-7132.
- Xie, S.-P., H. Annamalai, F. A. Schott, J. P. McCreary, 2002: Structure and mechanisms of South Indian Ocean climate variability. *J. Climate*, **15**, 864-878.
- Yu, L., R. A. Weller, and W. T. Liu, 2003: Case analysis of a role of ENSO in regulating the generation of westerly wind bursts in the western equatorial Pacific. *J. Geophys. Res.* **108**, **C4**, 3128, doi:10.1029/2002JC001498.

Figure lists

Fig. 1. A schematic diagram illustrating the neural network model used for performing NLPCA. The model is a feed-forward multi-layer perceptron neural network, with 3 'hidden' layers of variables or 'neurons' (denoted by circles) sandwiched between the input layer \mathbf{x} on the left and the output layer \mathbf{x}' on the right. Next to the input layer is the 'encoding' layer, followed by the narrow 'bottleneck' layer, then the 'decoding' layer, and finally the output layer, i.e. a total of 4 layers of transfer functions are needed to map from the inputs to the outputs. A neuron v_i at the i^{th} layer receives its value from the neurons \mathbf{v}_{i-1} in the preceding layer, i.e. $v_i = f_i(\mathbf{w}_i \cdot \mathbf{v}_{i-1} + b)$, where \mathbf{w}_i is a vector of weight parameters and b a bias parameter, and the transfer functions f_1 and f_3 are the hyperbolic tangent functions, while f_2 and f_4 are simply the identity functions. The bottleneck contains two neurons p and q constrained to lie on a unit circle, i.e. only 1 degree of freedom as represented by the angle θ . Effectively, a nonlinear function $\theta = f(\mathbf{x})$ maps from the higher dimension input space to the lower dimension bottleneck space, followed by an inverse transform $\mathbf{x}' = \mathbf{G}(\theta)$ mapping from the bottleneck space back to the original space, as represented by the outputs. To make the outputs as close to the inputs as possible, the cost function $J = \langle |\mathbf{x} - \mathbf{x}'|^2 \rangle$ (i.e. the mean square error, MSE) is minimized (where $\langle \dots \rangle$ denotes a sample or time mean). By minimizing J , the optimal values of the weight and bias parameters are solved. Data

compression is achieved by the bottleneck, yielding the nonlinear principal component (NLPC) θ .

Fig. 2. The 20 °C isotherm depth patterns of EOF1 (a) and EOF2 (b), and the corresponding principal component (PC) time series. The red solid line in each panel indicates the Nino-3 SST anomalies.

Fig. 3. Scatter plot of the thermocline anomaly data (dots) and the NLPCA mode 1 in the (a) PC1-PC2 plane, (b) 3-dimensional PC1-PC2-PC3 space. The NLPCA mode 1 approximation to the data is shown by the small circles, which traced out a closed curve. The progression of the system with time is primarily clockwise along the curve.

Fig. 4. Thermocline field for the (a) mature phase of El Niño, (b) transition phase from El Niño to La Niña, (c) mature phase of La Niña, and (d) transition phase from La Niña to El Niño. Contour interval is 5 m. Positive values are shaded.

Fig. 5. Phase-longitude section of the thermocline anomaly (in color; m) and the zonal wind stress anomaly (in contour; $\times 10^{-1} \text{ N m}^{-2}$) along the equator (5°S - 5°N) associated with the first mode NLPCA. Phase in y-axis represents the time sequence. Two cycles are plotted with the phase (in degrees) increasing with time.

Fig. 6. Phase-latitude section of the zonal-mean thermocline anomaly associated with the first mode NLPCA. Contour interval is 3 m. Positive values are shaded.

Fig. 7. Scatter plot of the thermocline anomaly data in PC1-PC2 plane, (a) for total period, (b) for pre-1980s only, and (c) for post-1980s only. Thermocline anomaly is obtained from the SODA data. The system progresses primarily clockwise along the curves.

Fig. 8. Phase-longitude section of the thermocline anomaly (in color; m) and the zonal wind stress anomaly (in contour; $\times 10^{-1} \text{ N m}^{-2}$) along the equator (5°S - 5°N) associated with the first mode NLPCA, (a) for total data period, (b) for pre-1980s only, and (c) for post-1980s only. Phase in y-axis represents the time sequence.

Fig. 9. Phase-latitude section of the zonal-mean thermocline anomaly associated with the first mode NLPCA, (a) for total period, (b) for pre-1980s only, and (c) for post-1980s only. Contour interval is 3 m. Positive values are shaded.

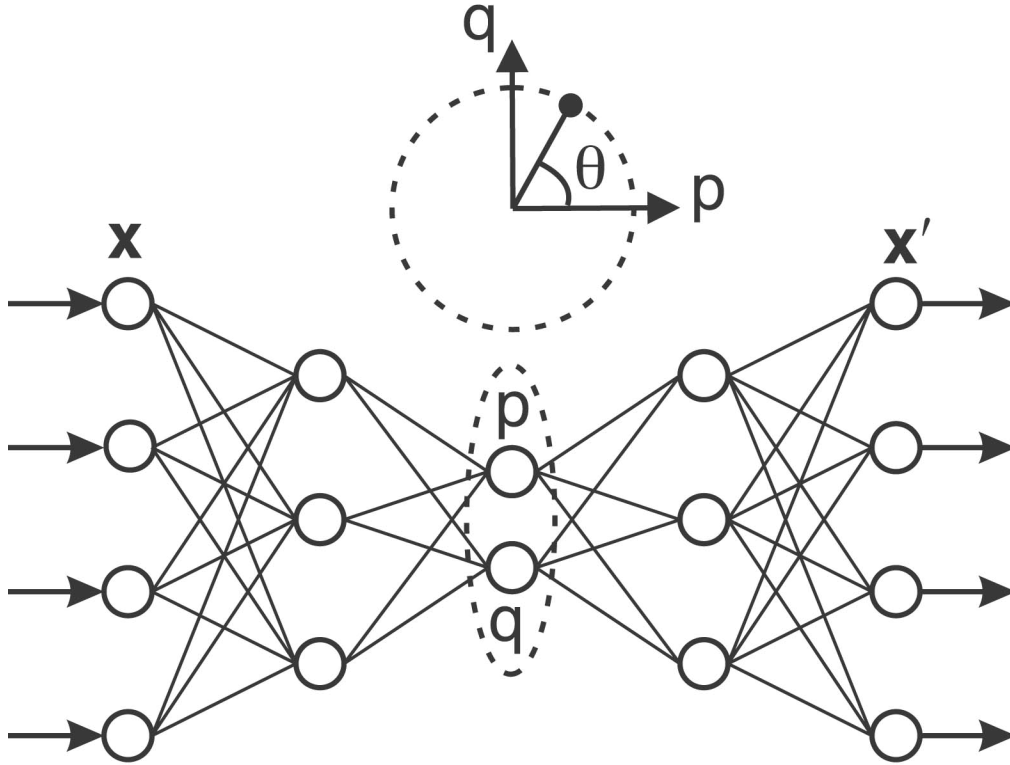


Fig. 1. A schematic diagram illustrating the neural network model used for performing NLPCA. The model is a feed-forward multi-layer perceptron neural network, with 3 ‘hidden’ layers of variables or ‘neurons’ (denoted by circles) sandwiched between the input layer \mathbf{x} on the left and the output layer \mathbf{x}' on the right. Next to the input layer is the ‘encoding’ layer, followed by the narrow ‘bottleneck’ layer, then the ‘decoding’ layer, and finally the output layer, i.e. a total of 4 layers of transfer functions are needed to map from the inputs to the outputs. A neuron v_i at the i^{th} layer receives its value from the neurons \mathbf{v}_{i-1} in the preceding layer, i.e. $v_i = f_i(\mathbf{w}_i \cdot \mathbf{v}_{i-1} + b)$, where \mathbf{w}_i is a vector of weight parameters and b a bias parameter, and the transfer functions f_1 and f_3 are the hyperbolic tangent functions, while f_2 and f_4 are simply the identity functions. The bottleneck contains two neurons p and q constrained to lie on a unit circle, i.e. only 1 degree of freedom as represented by the angle θ . Effectively, a nonlinear function $\theta = f(\mathbf{x})$ maps from the higher dimension input space to the lower dimension bottleneck space, followed by an inverse transform $\mathbf{x}' = \mathbf{G}(\theta)$ mapping from the bottleneck space back to the original space, as represented by the outputs. To make the outputs as close to the inputs as possible, the cost function $J = \langle |\mathbf{x} - \mathbf{x}'|^2 \rangle$ (i.e. the mean square error, MSE) is minimized (where $\langle \dots \rangle$ denotes a sample or time mean). By minimizing J , the optimal values of the weight and bias parameters are solved. Data compression is achieved by the bottleneck, yielding the nonlinear principal component (NLPC) θ .

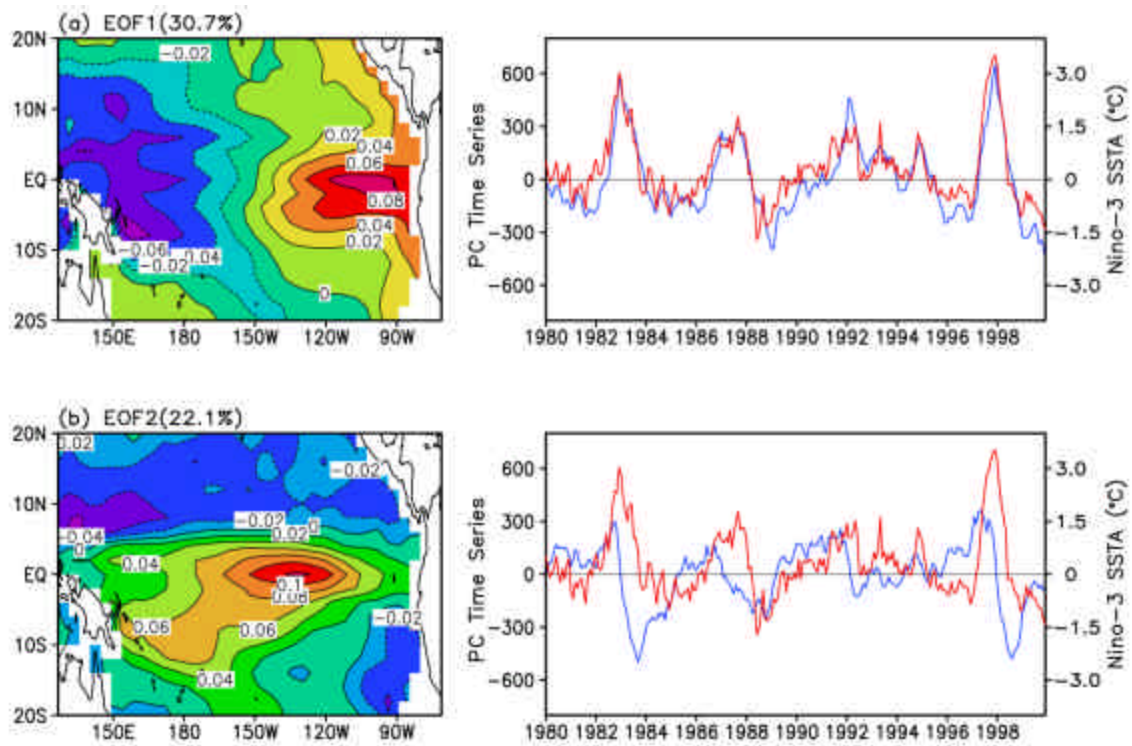


Fig. 2. The 20 °C isotherm depth patterns of EOF1 (a) and EOF2 (b), and the corresponding principal component (PC) time series. The red solid line in each panel indicates the Nino-3 SST anomalies.

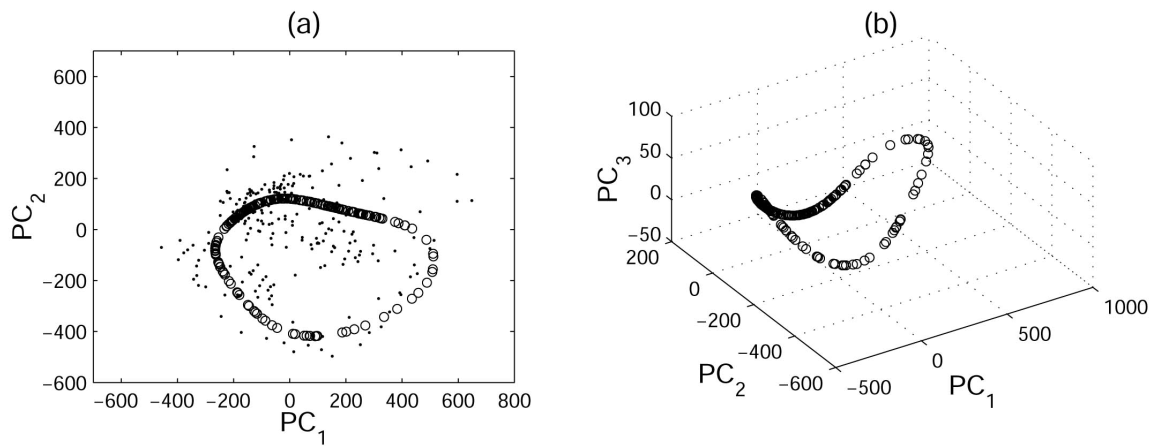


Fig. 3. Scatter plot of the thermocline anomaly data (dots) and the NLPCA mode 1 in the (a) PC1-PC2 plane, (b) 3-dimensional PC1-PC2-PC3 space. The NLPCA mode 1 approximation to the data is shown by the small circles, which traced out a closed curve. The progression of the system with time is primarily clockwise along the curve.

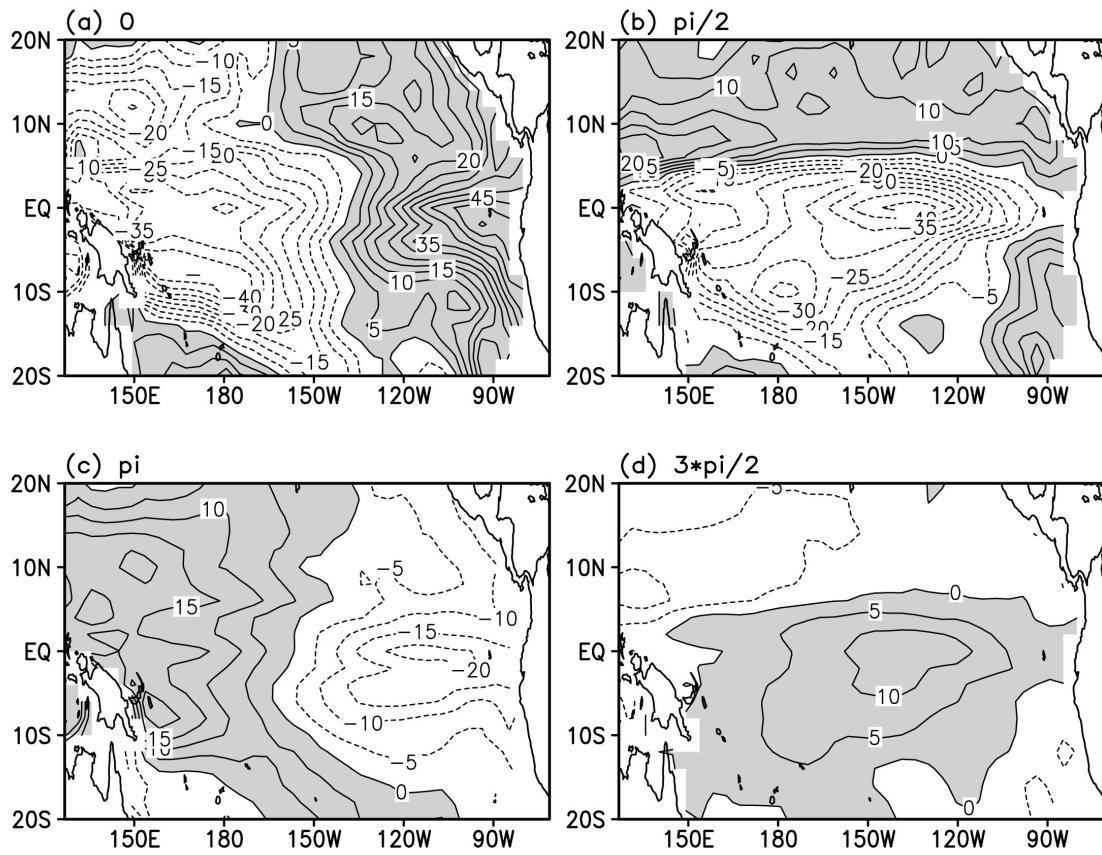


Fig. 4 Thermocline field for the (a) mature phase of El Niño, (b) transition phase from El Niño to La Niña, (c) mature phase of La Niña, and (d) transition phase from La Niña to El Niño. Contour interval is 5 m. Positive values are shaded.

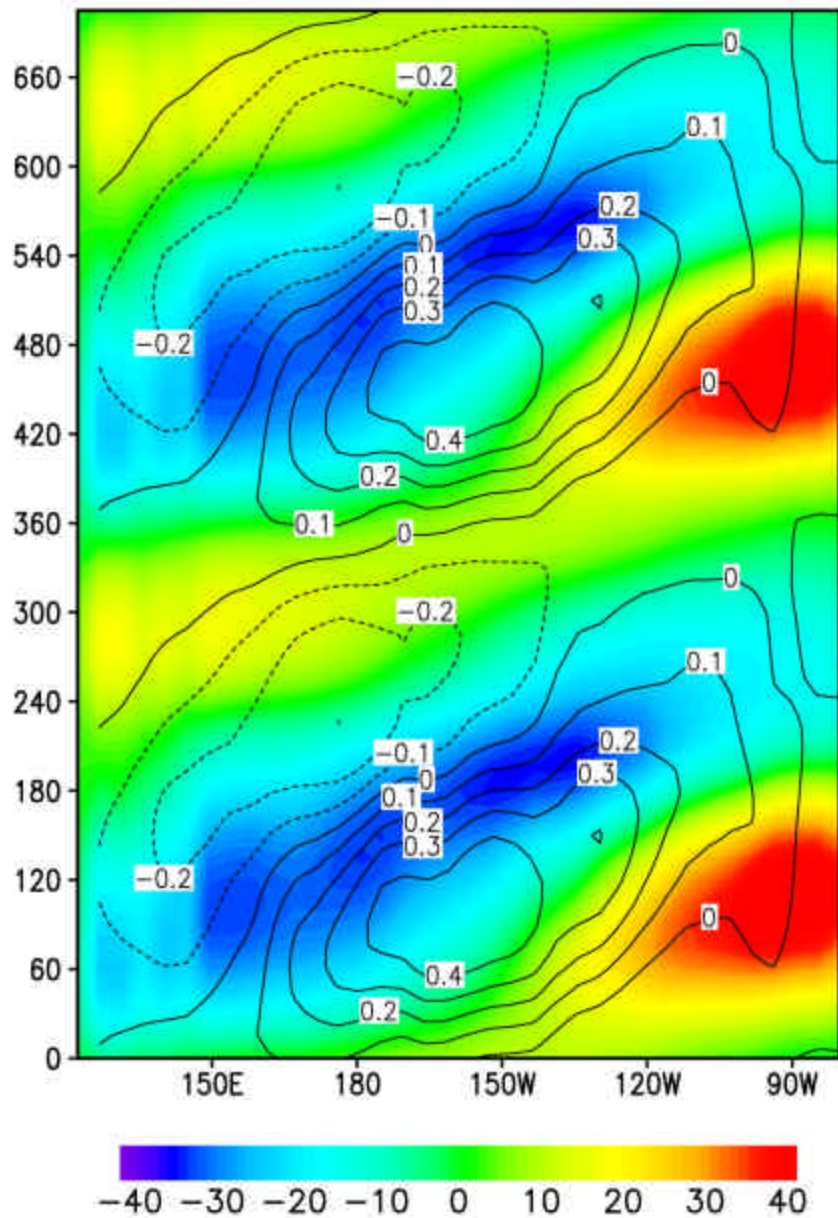


Fig. 5. Phase-longitude section of the thermocline anomaly (in color; m) and the zonal wind stress anomaly (in contour; $\times 10^{-1} \text{ N m}^{-2}$) along the equator (5°S - 5°N) associated with the first mode NLPCA. Phase in y-axis represents the time sequence. Two cycles are plotted with the phase (in degrees) increasing with time.

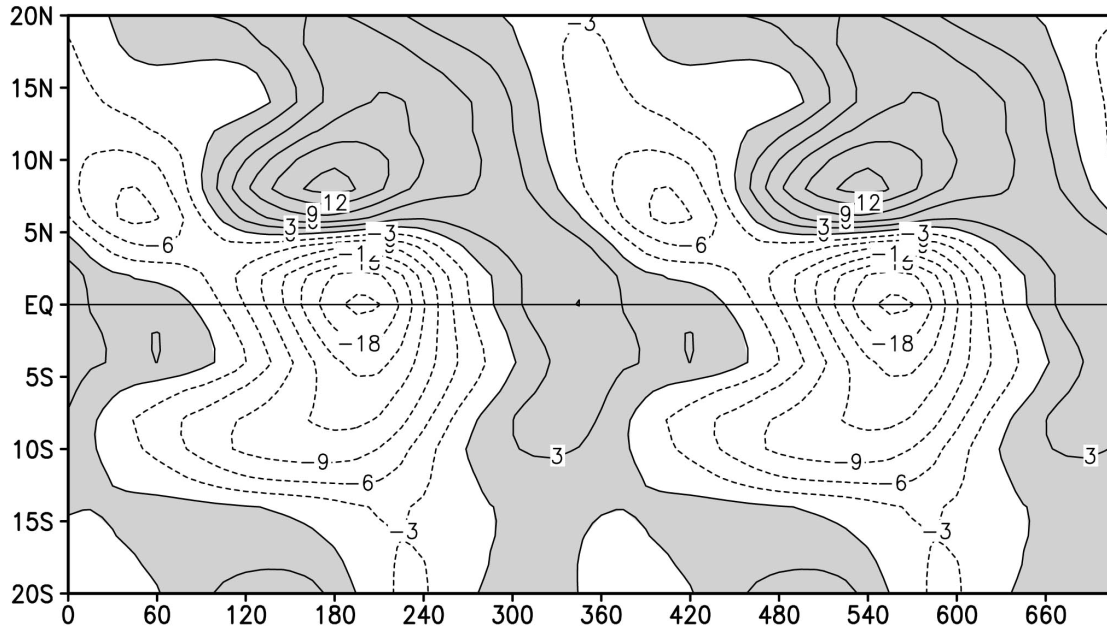


Fig. 6. Phase-latitude section of the zonal-mean thermocline anomaly associated with the first mode NLPCA. Contour interval is 3 m. Positive values are shaded.

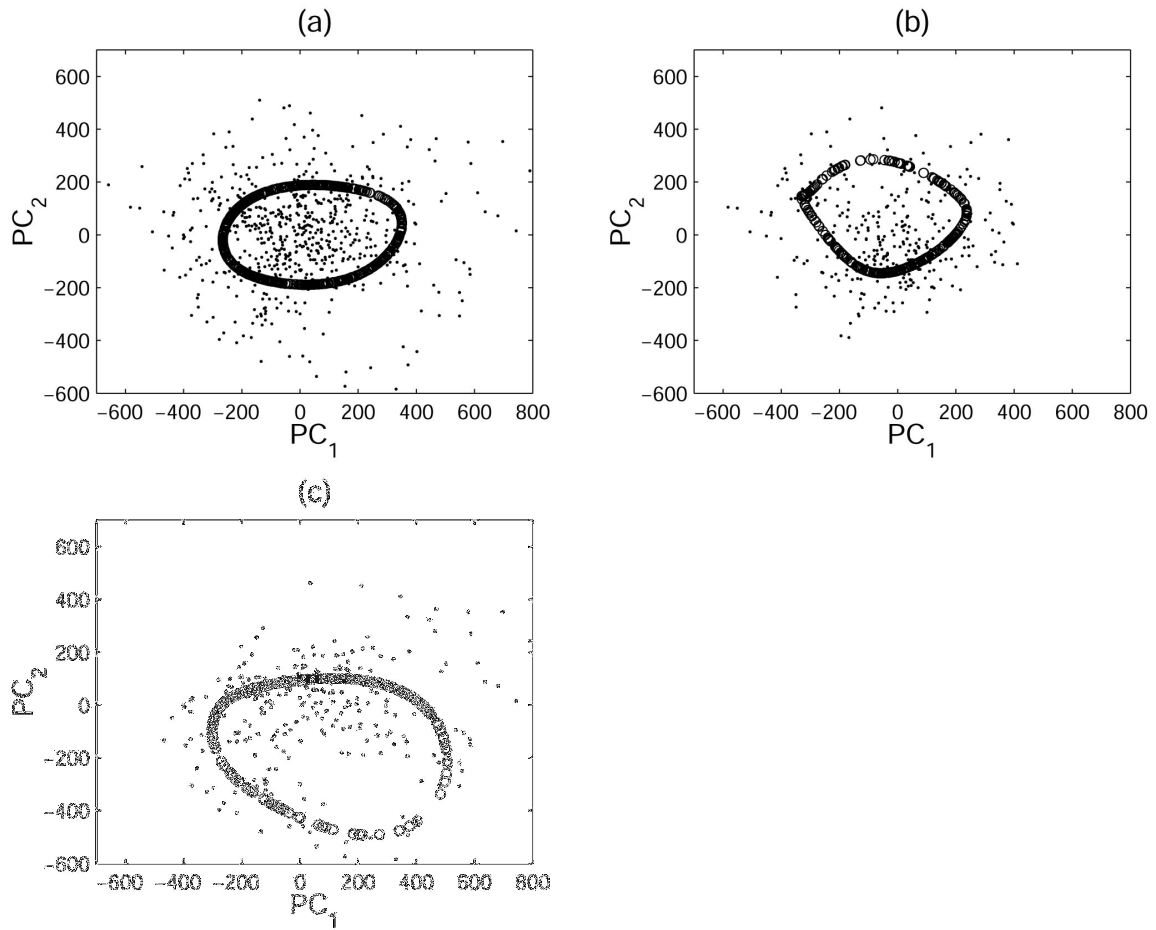


Fig. 7. Scatter plot of the thermocline anomaly data in PC1-PC2 plane, (a) for total period, (b) for pre-1980s only, and (c) for post-1980s only. Thermocline anomaly is obtained from the SODA data. The system progresses primarily clockwise along the curves.

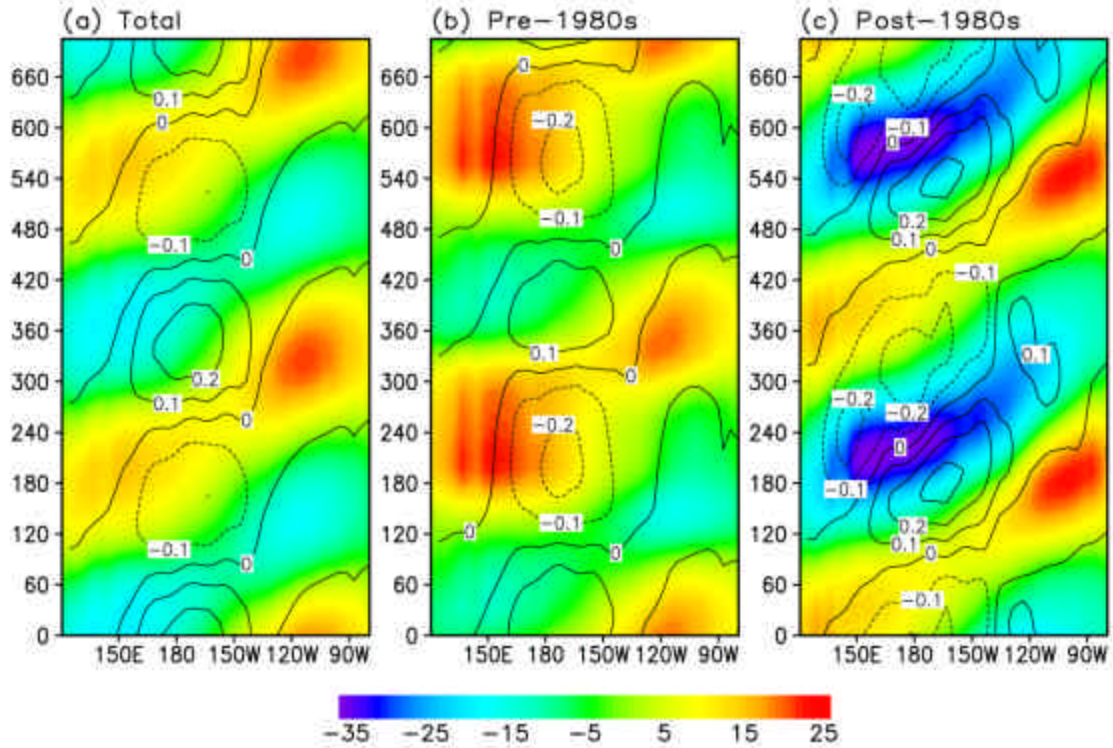


Fig. 8. Phase-longitude section of the thermocline anomaly (in color; m) and the zonal wind stress anomaly (in contour; $\times 10^{-1} \text{ N m}^{-2}$) along the equator (5°S - 5°N) associated with the first mode NLPCA, (a) for total data period, (b) for pre-1980s only, and (c) for post-1980s only. Phase in y-axis represents the time sequence.

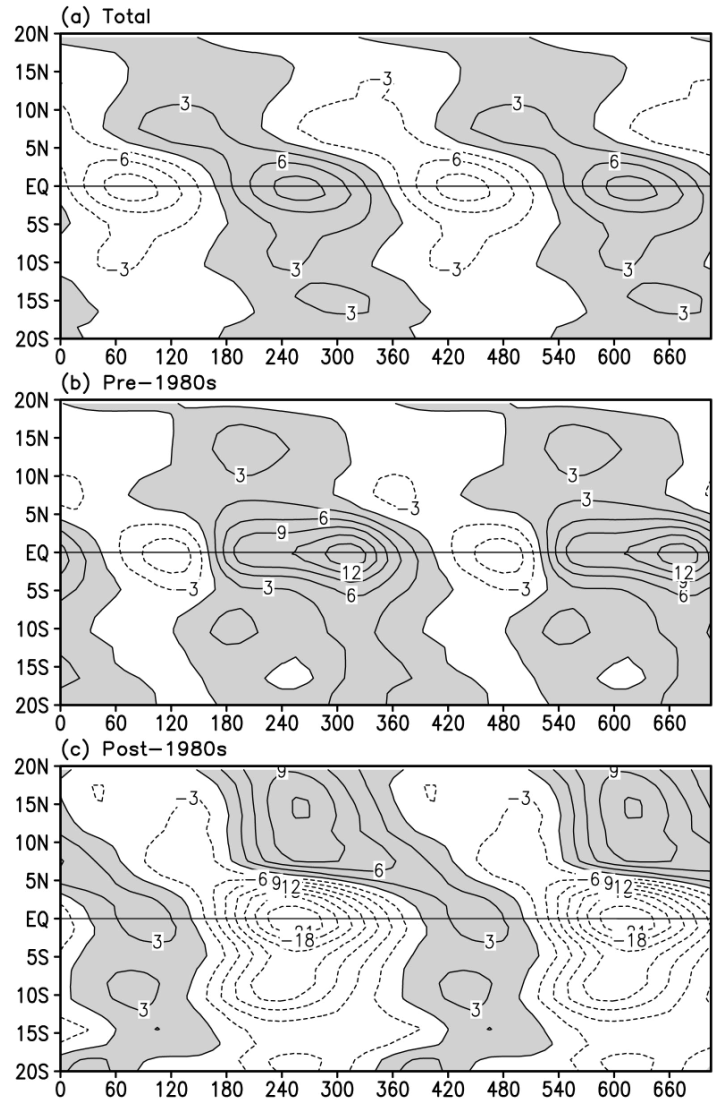


Fig. 9. Phase-latitude section of the zonal-mean thermocline anomaly associated with the first mode NLPCA, (a) for total period, (b) for pre-1980s only, and (c) for post-1980s only. Contour interval is 3 m. Positive values are shaded.